E-ISSN: 2948-5231

Article

Journal of Asian Geography, 2026, Volume 5 (Issue 2), 18-24
https://doi.org/10.36777/jag2026.5.2.2

GIS-Based Flood Risk Assessment in the Johor River Basin Using AHP and Weighted Overlay

Zhang Yibo[1], and Mohd Amirul Mahamud[1,*]

[1] Geography Section, School of Humanities, Universiti Sains Malaysia, 11800 USM, Penang, Malaysia.

*Correspondence: mohd.amirul@usm.my

Received: 16 May 2026, Revised: 18 Aug 2026; Accepted: 27 Aug 2026; Published 29 Sep 2026

Abstract: Flood-risk studies in Malaysia have often concentrated on hydrological hazard, although the consequences of flooding also depend on where people and assets are located and how well communities can cope. This study develops a basin-wide flood-risk index for the Johor River Basin by integrating hazard, exposure and vulnerability within a geographic information system-based multi-criteria decision analysis. Nine hazard indicators, four exposure indicators and four vulnerability indicators were assembled from open geospatial datasets. The indicators were standardised into five ordinal classes, weighted using the Analytic Hierarchy Process, and combined through weighted overlay. The three component indices were then assigned equal weights to produce a composite flood-risk surface. High and very high risk covered 9.29% and 1.43% of the basin, respectively. These areas were concentrated around Kota Tinggi in the lower basin and, in smaller clusters, around Bandar Tenggara in the middle basin. A spatial consistency check used 24 locations listed in a Department of Irrigation and Drainage flood warning for 14-17 December 2025. Nineteen locations (79.17%) fell within high or very high risk classes, while 23 (95.83%) fell within moderate to very high classes. The resulting map is best interpreted as a relative screening tool for prioritising detailed investigation, land-use control and preparedness. Its main limitations are the use of mixed-date datasets, subjective weighting, a climatological rainfall surface, and the absence of hydrodynamic simulation and observed inundation footprints.

Keywords: Analytic hierarchy process; flood risk; geographic information system; Johor River Basin; multi-criteria decision analysis

1.0 Introduction

Flooding is among the most persistent environmental hazards in Southeast Asia. Monsoonal rainfall, low-lying settlements and rapid urban growth create conditions in which a hydrological event can quickly become a social and economic emergency. Climate change adds a further layer of concern because warmer conditions can intensify the hydrological cycle and alter the frequency and magnitude of river flooding (Hirabayashi et al., 2013). Yet hazard alone does not determine disaster losses. The same flood can produce very different outcomes depending on the concentration of people and assets in its path, the sensitivity of affected communities and their capacity to prepare, respond and recover (United Nations Office for Disaster Risk Reduction [UNDRR], 2022).

This distinction matters in Malaysia, where flood research and practice have traditionally placed strong emphasis on rainfall-runoff processes, river hydraulics and engineering control. Such work is indispensable for understanding water movement, but it can leave the geography of consequences less explicit. National reviews have also identified fragmented responsibilities, uneven communication and difficulties translating risk information into coordinated action (Muzamil et al., 2022; Rosmadi et al., 2023). Spatially integrated assessments can complement hydraulic studies by showing where unfavourable physical conditions coincide with dense settlement, infrastructure and socially vulnerable groups.

The Johor River Basin illustrates this need. It contains rapidly developing urban areas, agricultural land and important water-supply infrastructure, while remaining exposed to heavy northeast-monsoon rainfall. Existing basin research has produced valuable hydrological evidence. Tan et al. (2015), for example, found that land-use change exerted a strong influence on hydrological behaviour in the basin, and broader reviews show that Malaysian studies remain dominated by runoff simulation and hazard modelling (Abdulkareem et al., 2018). Detailed hydraulic modelling has also improved understanding of urban inundation and the performance of mitigation measures in Malaysia (Sidek et al., 2021). However, fewer studies have mapped hazard, exposure and vulnerability together across the full Johor River Basin using a consistent spatial framework.

Geographic information systems (GIS) and multi-criteria decision analysis (MCDA) offer a practical way to address this gap when comprehensive flood-depth, damage and household-level data are unavailable. GIS supports the alignment and overlay of heterogeneous spatial layers, while MCDA makes the assumptions used to combine them visible and reproducible (Malczewski, 2006). The Analytic Hierarchy Process (AHP) is frequently paired with GIS because it converts pairwise judgements into criterion weights and includes a formal consistency test (Saaty, 1980). AHP-based flood mapping has been applied across different environmental settings, particularly where data scarcity limits physically based modelling (Kazakis et al., 2015; Souissi et al., 2020). Its accessibility is also its main weakness: weights and class boundaries reflect analytical judgement, so the resulting surface represents relative priority rather than an event probability or predicted inundation depth (de Brito & Evers, 2016).

Against this background, the present study develops an integrated, basin-wide flood-risk index for the Johor River Basin. Three objectives guide the analysis: (1) to represent flood hazard, exposure and vulnerability using openly available geospatial indicators; (2) to combine those indicators through an AHP-weighted GIS framework; and (3) to identify priority areas and assess their spatial agreement with locations included in a recent official flood warning. The study contributes a current spatial screening perspective and pays particular attention to risk outside the commonly recognised downstream hotspot of Kota Tinggi.

2.0 Study Area

The Johor River Basin lies in southern Peninsular Malaysia and covers approximately 2,636 km² (Figure 1). The main river is about 123 km long, rising near Mount Gemuruh and flowing generally southwards into the Johor Strait (UNESCO Regional Office for Science and Technology for Southeast Asia, 1997). The basin encompasses forest, agricultural land and expanding settlements, including Kota Tinggi in the lower basin and Bandar Tenggara farther upstream. It also supports strategically important water-supply functions for Johor and Singapore.

Rainfall is strongly seasonal. The northeast monsoon, usually extending from November to March, brings prolonged and sometimes intense rainfall to eastern Johor. The basin's topography changes from higher ground in the north and north-west to lower-gradient terrain downstream, where runoff converges and settlements occupy flood-prone land. Urban expansion adds impervious surfaces and concentrates population, buildings and roads in locations where physical susceptibility may already be high. These linked environmental and development pressures make a basin-wide assessment more informative than a study confined to municipal boundaries.

Article Journal of Asian Geography, 2026, Volume 5 (Issue 2), 18-24
https://doi.org/10.36777/jag2026.5.2.2
E-ISSN: 2948-5231

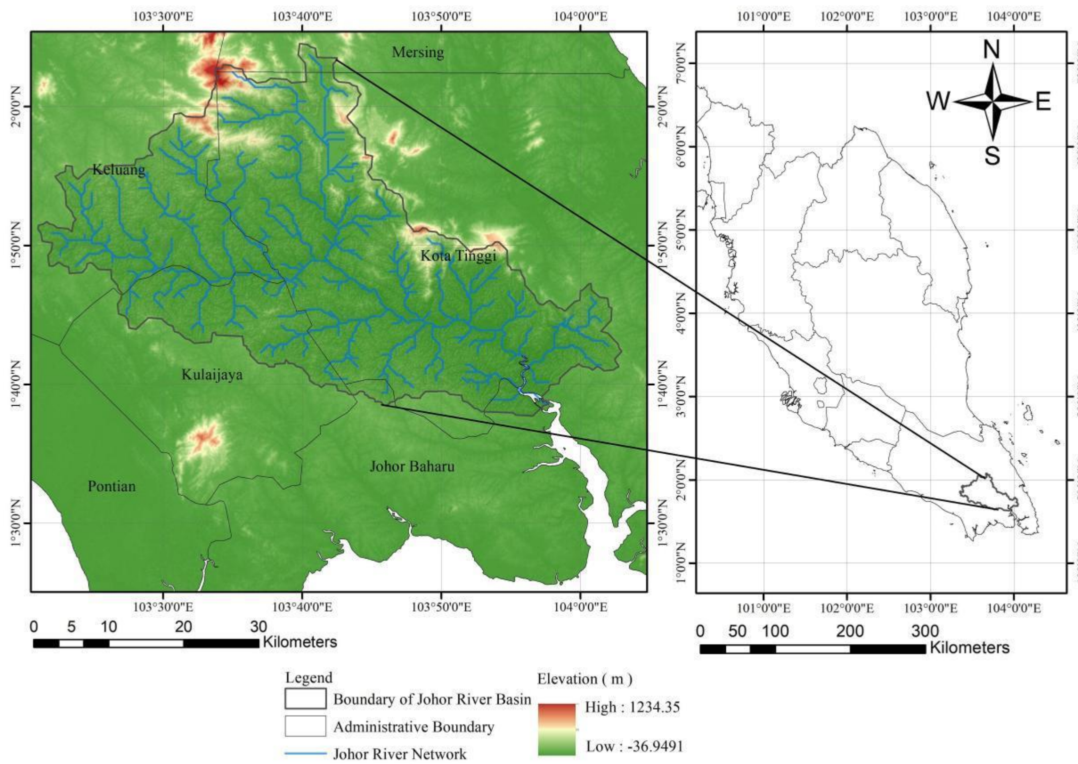

Figure 1: Location, elevation and drainage network of the Johor River Basin.

3.0 Materials and Methodology

3.1 Conceptual framework

Risk was treated as the spatial interaction of hazard, exposure and vulnerability. Hazard describes the physical conditions that favour flood occurrence or accumulation; exposure represents the people, buildings, infrastructure and land assets located in potentially affected areas; and vulnerability represents characteristics that may increase susceptibility or constrain coping capacity. The output is therefore a relative composite index. It does not estimate an annual exceedance probability, flood depth, flow velocity or monetary loss.

The workflow comprised six stages: indicator selection, data acquisition, spatial preprocessing, indicator standardisation, AHP weighting and weighted overlay, followed by a spatial consistency check. All layers were clipped to the basin and brought into a common GIS environment using WGS 1984 UTM Zone 48N. The analysis grid was aligned at 30 m for overlay, although the native resolution of each source dataset was retained in the methodological record because it determines the effective information content of the final map.

3.2 Indicators and spatial preprocessing

Seventeen component-specific indicators were used: nine for hazard, four for exposure and four for vulnerability (Table 1). Some underlying datasets served more than one conceptual role. Land cover, for instance, represented infiltration and runoff behaviour in the hazard component but served as a proxy for asset concentration in the exposure component. The Normalized Difference Vegetation Index (NDVI) reflected interception and infiltration in the hazard component and ecological sensitivity in the vulnerability component. These repeated uses were retained because their direction and meaning differed between components:

Table 1: Indicators, source datasets, native resolution and AHP weights.

Component	Indicator	Dataset and reference year	Native resolution	AHP weight (%)
Hazard	Precipitation	WorldClim 2.1 normals (1970-2000)	~1 km	33.52
Hazard	Slope	Derived from Copernicus DEM GLO-30	30 m	11.17
Hazard	Elevation	Copernicus DEM GLO-30 (release 2021)	30 m	11.17
Hazard	Land cover	ESA WorldCover v200 (2021)	10 m	6.70
Hazard	NDVI	MODIS MOD13Q1 (December 2024)	250 m	5.59
Hazard	Flow accumulation	Derived from Copernicus DEM GLO-30	30 m	8.38
Hazard	Drainage density	HydroRIVERS (release 2013)	Vector to 30 m	8.38
Hazard	Proximity to river	HydroRIVERS (release 2013)	Vector to 30 m	8.38
Hazard	Soil type	Harmonized World Soil Database v2.0 (2023)	~1 km	6.70

Component	Indicator	Dataset and reference year	Native resolution	AHP weight (%)
Exposure	Population density	WorldPop population density (2020)	~1 km	42.86
Exposure	Building density	Google Open Buildings (release 2023)	Vector to 30 m	21.43
Exposure	Land cover	ESA WorldCover v200 (2021)	10 m	21.43
Exposure	Road density	OpenStreetMap (accessed 1 December 2025)	Vector to 30 m	14.29
Vulnerability	Nighttime light radiance	VIIRS monthly DNB composites (2024 mean)	~500 m	44.44
Vulnerability	Children aged <=9 years	WorldPop age-sex structures (2024)	100 m	22.22
Vulnerability	Adults aged >=60 years	WorldPop age-sex structures (2024)	100 m	22.22
Vulnerability	NDVI	MODIS MOD13Q1 (December 2024)	250 m	11.11

Elevation was obtained from the Copernicus GLO-30 digital surface model. Slope and flow accumulation were derived from this layer; flow accumulation was transformed as log10(contributing cells + 1) to reduce the influence of extreme values while preserving drainage pathways. Mean annual precipitation was calculated by summing the 12 monthly WorldClim 2.1 precipitation normals for 1970-2000 (Fick & Hijmans, 2017). The 2021 ESA WorldCover product represented land cover at 10 m resolution (Zanaga et al., 2022), while a December 2024 MODIS MOD13Q1 scene supplied NDVI (Didan, 2015). Drainage density and Euclidean distance to rivers were derived from HydroRIVERS (Lehner & Grill, 2013), and soil classes were obtained from the Harmonized World Soil Database version 2.0.

Exposure was represented by total population density, building density, land cover and road density. Population density was obtained from WorldPop. Google Open Buildings footprints were converted to a GIS feature layer and summarised using kernel density estimation (Sirko et al., 2021). Roads were extracted from OpenStreetMap on 1 December 2025 and converted to a line-density surface (OpenStreetMap contributors, 2025).

Vulnerability combined the density of children aged nine years or younger, the density of adults aged 60 years or older, NDVI and nighttime light radiance. The two age-group surfaces were aggregated from WorldPop age-sex grids. Children and older adults were assigned increasing vulnerability scores as their density rose because evacuation, mobility and access to information can be more constrained for these groups. Monthly VIIRS Day/Night Band composites for 2024 were averaged to represent nighttime light radiance (Elvidge et al., 2021). This indicator was interpreted as a proxy for economic activity and coping capacity, so lower radiance received a higher vulnerability score. This inverse interpretation is important because nighttime lights can also represent asset exposure; the implications are revisited in the discussion.

3.3 *Standardisation and AHP weighting*

Continuous indicators were divided into five ordinal classes using Jenks natural breaks and assigned scores from 1 (very low contribution) to 5 (very high contribution). The direction of scoring followed the conceptual relationship with each component. Higher precipitation, flow accumulation and drainage density increased hazard scores, whereas higher elevation, steeper slope, greater distance from a river and denser vegetation reduced them. Population, buildings and roads were positively related to exposure. Densities of children and older adults were positively related to vulnerability, while NDVI and nighttime light radiance were inversely scored.

Categorical land-cover and soil layers were ranked manually. Built-up and bare surfaces received the highest hazard score, followed by cropland, shrubland, grassland and tree cover; wetlands, permanent water and mangroves received the lowest score because of their storage or buffering functions in the adopted framework. For exposure, built-up land received the highest score, cropland the next highest, and water, wetlands, mangroves and sparse vegetation the lowest. Tree cover was assigned an intermediate exposure score because the WorldCover class does not distinguish primary forest from economically valuable oil-palm and rubber plantations.

AHP pairwise comparison matrices were constructed separately for hazard, exposure and vulnerability using evidence from the flood-mapping literature and the local environmental context. For a matrix A = [a_ij], the normalised principal eigenvector provided the criterion weights. Consistency was evaluated using CI = (lambda_max - n)/(n - 1) and CR = CI/RI, where RI is Saaty's random index. All three matrices produced CR = 0.00 because the comparisons were constructed as reciprocal, strictly transitive ratios. This confirms mathematical consistency, although it does not remove the substantive uncertainty associated with selecting the judgements themselves.

For each component d, the index was calculated using a weighted linear combination:

$$I\_d = \mathrm{sum}(w\_di \times s\_di)$$

where w_di is the AHP weight of indicator i in component d and s_di is its standardised score. The highest hazard weight was assigned to precipitation (33.52%). Population density dominated exposure (42.86%), while nighttime light radiance carried the largest vulnerability weight (44.44%). The component indices were each classified into five levels using natural breaks.

3.4 *Standardisation and AHP weighting*

The final risk surface was produced through an equal-weighted overlay of the three component indices:

$$R = 0.3334H + 0.3333E + 0.3333V$$

where H, E and V are the hazard, exposure and vulnerability indices. The slightly different fourth decimal for H ensured that the implemented weights summed to one. The composite values were classified into very low, low, moderate, high and very high-risk using Jenks natural breaks.

Historical inundation polygons suitable for independent receiver operating characteristic or area-under-the-curve analysis were unavailable. A point-overlay assessment was therefore conducted using 24 low-lying locations listed in a Department of Irrigation and Drainage warning for flooding expected between 14 and 17 December 2025 (Shadiqe, 2025). For a selected threshold c, spatial consistency was calculated as:

$$SC\_c = (\text{number of warning locations in class c or higher} / 24) \times 100.$$

E-ISSN: 2948-5231
Article Journal of Asian Geography, 2026, Volume 5 (Issue 2), 18-24
https://doi.org/10.36777/jag2026.5.2.2

Two thresholds were reported: high or higher as a strict screening threshold, and moderate or higher as a broader coverage threshold. Because the locations came from a warning rather than a mapped record of observed inundation, this procedure should be interpreted as a plausibility check, not as a conventional predictive validation.

4.0 Results

4.1 Hazard, exposure and vulnerability patterns

The hazard surface displayed a broad north-east to south-west contrast and a pronounced corridor through the middle and lower basin (Figure 2a). Higher hazard scores occurred where heavier climatological rainfall coincided with low elevation, gentle slopes, convergent flow and dense drainage. The lower basin around Kota Tinggi was prominent, but elevated hazard also extended through parts of the middle basin. Urban and sparsely vegetated surfaces increased the local score by reducing the assumed capacity for infiltration and storage.

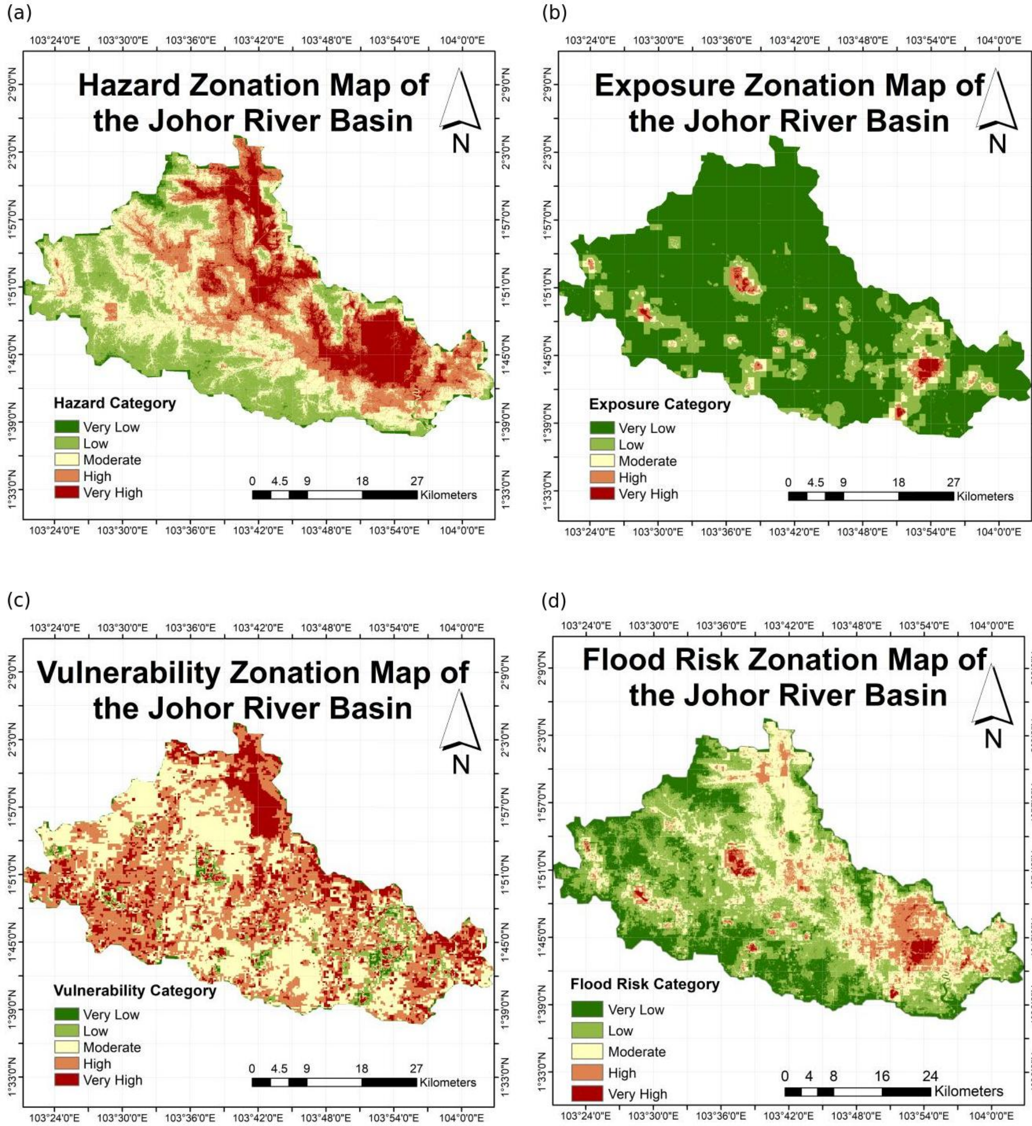

Figure 2: Spatial distribution of (a) flood hazard, (b) exposure, (c) vulnerability and (d) composite flood risk in the Johor River Basin.

Exposure was much more spatially concentrated than hazard (Figure 2b). Most of the basin remained in the very low or low exposure classes, while distinct high-exposure clusters appeared around Kota Tinggi, Bandar Tenggara and several smaller settlements. The pattern closely followed population and building density, which together accounted for 64.29% of the exposure weights. Road density and the exposure ranking of built-up land reinforced these urban clusters.

The vulnerability map differed from both hazard and exposure (Figure 2c). Higher values appeared across several rural and peri-urban areas, whereas the brightest urban cores tended to receive lower vulnerability scores. This pattern followed the inverse scoring of nighttime light radiance, which contributed 44.44% of the vulnerability index. Areas with low radiance but appreciable concentrations of children or older adults were consequently elevated. The result identifies possible capacity constraints, but it should not be read as a direct measure of household deprivation without local socioeconomic data.

E-ISSN: 2948-5231
Article
Journal of Asian Geography, 2026, Volume 5 (Issue 2), 18-24
https://doi.org/10.36777/jag2026.5.2.2

4.2 Composite flood-risk distribution

The composite risk surface combined the extensive physical-hazard corridor with the more localised exposure and vulnerability patterns (Figure 2d). Low risk formed the largest class, covering 38.35% of the basin, followed by moderate risk at 29.42% and very low risk at 21.51% (Table 2). High risk accounted for 9.29%, while very high risk represented 1.43%. Together, the two upper classes covered 10.72% of the basin.

Table 2: Area share and flood-warning locations by composite risk class.

Risk class	Basin area (%)	Warning locations (n)	Warning locations (%)
Very low	21.51	0	0.00
Low	38.35	1	4.17
Moderate	29.42	4	16.67
High	9.29	7	29.17
Very high	1.43	12	50.00

Very high risk was concentrated mainly in and around Kota Tinggi. Here, downstream hydrological convergence overlaps with dense settlement, buildings and roads. The high-risk class formed a wider zone around this core and extended into nearby developed land. Smaller high and very high-risk patches also occurred around Bandar Tenggara and at scattered locations in the middle basin. These mid-basin clusters are important because they sit outside the best-known downstream hotspot yet combine urban exposure with locally unfavourable terrain and flow-accumulation conditions.

4.3 Composite flood-risk distribution

Of the 24 locations included in the December 2025 flood warning, 12 fell in the very high-risk class and seven in the high class. Four were classified as moderate, one as low and none as very low (Figure 3). The strict high-or-higher consistency rate was therefore 79.17% (19/24), while the moderate-or-higher rate reached 95.83% (23/24). The concentration of warning locations in the upper risk classes supports the spatial plausibility of the screening surface. However, the result reflects one warning period and a point representation of named locations; it does not quantify inundated area, false-positive cells or performance across different flood magnitudes.

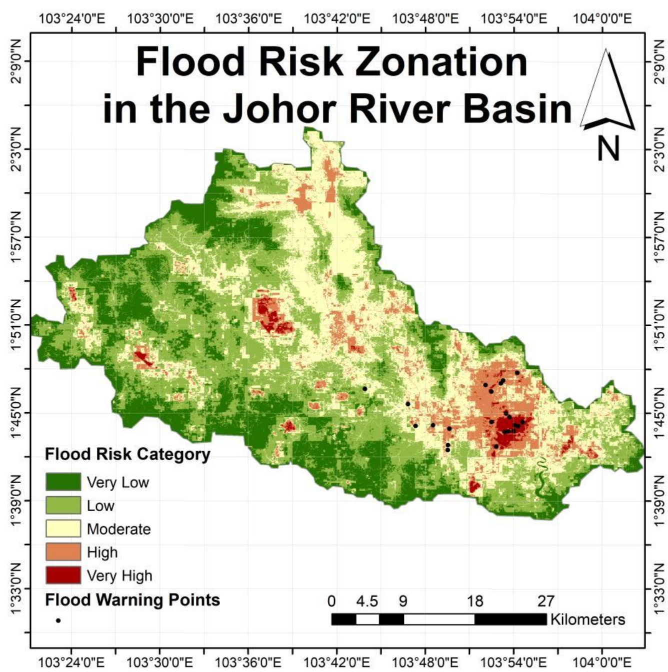

Figure 3: Composite flood-risk classes and the 24 locations included in the 14-17 December 2025 flood warning.

5.0 Discussion

5.1 Interpreting the basin-wide pattern

The analysis reveals a risk geography shaped by the coincidence of physical susceptibility and development. Kota Tinggi emerges clearly because the lower basin accumulates runoff while also containing a dense concentration of people and assets. This finding is consistent with hydrological research showing that land-use change has materially affected runoff behaviour in the Johor River Basin (Tan et al., 2015). It also supports the broader observation that growth in flood losses is often driven as much by increasing exposure as by changes in the hazard itself (Jongman et al., 2012; Ward et al., 2013).

The mid-basin clusters around Bandar Tenggara add a less obvious result. They are not as extensive as the lower-basin hotspot, but their appearance across independent hazard and exposure layers indicates that they should not be treated as isolated artefacts of a single criterion. This is the main value of the basin-wide perspective: administrative or town-centred studies can overlook corridors where runoff accumulation, expanding settlement and local vulnerability intersect outside established flood-management priorities.

The component maps also show why risk should not be inferred from any one layer. High hazard does not automatically produce high composite risk where population and assets are sparse. Conversely, high exposure in a better-drained or higher-elevation location may not translate into the highest risk class. The overlay makes these contrasts visible, but it remains a relative index. It ranks places against other locations within the basin and should not be interpreted as a probability that a particular property will flood.

5.2 Interpreting the basin-wide pattern

The upper risk classes provide a first-pass basis for prioritising more detailed work. In Kota Tinggi and the identified mid-basin clusters, planning agencies could use the map to screen development proposals before commissioning site-level topographic surveys and hydraulic modelling. New residential or critical-facility development should be approached cautiously where high exposure overlaps with low-lying land near rivers. Development controls are especially important because additional impervious cover can increase runoff while simultaneously placing more people and assets in harm's way.

For existing urban areas, the pattern points to a combination of structural and nature-based measures. Drainage capacity, culvert constraints and river conveyance require engineering assessment, while riparian setbacks, connected green space and retention areas can provide temporary storage and reduce the speed at which runoff reaches the channel. Such measures should be designed from field and hydraulic evidence rather than from the index alone. The map can help decide where that evidence should be collected first.

Preparedness is equally important. The strong overlap between warning locations and the moderate-to-very-high classes suggests that the index could support the spatial targeting of warning communication, evacuation planning and community education. High-risk neighbourhoods should receive clear, locally relevant information before the northeast monsoon, with particular attention to households that include young children, older adults or residents with limited mobility. Public InfoBanjir water-level information and meteorological warnings can be linked with local communication channels, but responsibilities for issuing, translating and acting on warnings must be explicit (Rosmadi et al., 2023).

5.3 Methodological uncertainty and limitations

Several choices constrain the strength of inference. First, the indicators come from different years and native resolutions. The precipitation surface is a 1970-2000 climatology, whereas several exposure and vulnerability layers describe 2020-2025. A 30 m output grid cannot create 30 m information from a 1 km source layer; it only aligns the layers for calculation. The fine visual texture of the final map should therefore not be mistaken for uniform fine-scale accuracy.

Second, AHP weights remain judgement-based. Perfect matrix consistency indicates that the ratios are mathematically coherent, not that the chosen priorities are empirically optimal. The vulnerability surface is particularly sensitive to the high weight and inverse scoring of nighttime light radiance. Nighttime lights may represent coping capacity, but they also correlate with asset concentration, infrastructure and urban form. Future work should compare alternative vulnerability specifications, incorporate income, disability, housing quality and access to services, and perform a formal weight-sensitivity analysis.

Third, the model does not simulate flood hydraulics. It omits event rainfall, channel cross-sections, floodplain storage, drainage-system capacity, water depth, velocity and duration. The hazard component is therefore closer to a susceptibility surface than an event-specific hazard model. Coupling this screening framework with HEC-RAS or another calibrated hydrodynamic model would provide a stronger physical representation of inundation and allow risk to be evaluated for defined return periods.

Fourth, the consistency assessment is limited. The 24 warning locations came from a single forecast period and do not constitute observed flood footprints. Point-overlay rates reward coverage of listed places but cannot assess the large number of map cells where flooding was not reported. A more rigorous evaluation would use multi-event inundation polygons, satellite-derived flood extents or verified damage records and would report discrimination, calibration and spatial error. Until such data are available, the present map should be used to prioritise investigation rather than to justify parcel-level regulatory decisions.

6.0 Conclusions

This study produced an integrated flood-risk screening map for the Johor River Basin using open geospatial data, AHP and weighted overlay. High and very high risk covered 9.29% and 1.43% of the basin, respectively, with the clearest concentration around Kota Tinggi and smaller but meaningful clusters around Bandar Tenggara and other mid-basin settlements. Nineteen of 24 locations in a December 2025 flood warning fell in the high or very high classes, and 23 fell in the moderate-to-very-high classes.

The map's practical contribution is its basin-wide comparison of where physical susceptibility coincides with people, assets and potential coping constraints. It can guide the targeting of hydraulic studies, drainage assessment, development screening, riparian protection and preparedness. At the same time, it is a relative index rather than a forecast of flood depth or probability. Future research should harmonise data dates, test alternative weights, incorporate locally grounded vulnerability variables, and validate the model against multiple observed inundation events. Integrating these improvements with hydrodynamic modelling would turn the present screening framework into a more robust basis for operational flood-risk management.

Acknowledgement: The authors acknowledge Universiti Sains Malaysia for supporting the research and the organisations that make the geospatial datasets used in this study openly available.

Conflicts of Interest: The authors declare no conflict of interest in this study

Data Availability: All source datasets used in the analysis are publicly accessible from the organisations identified in Table 1. The derived GIS layers may be made available by the corresponding author subject to the terms of the source-data licences.

Ethical approval: As the study is based on secondary data available in the public domain for research, no ethical approval was required from any institutional review board (IRB).

Funding: The authors received no financial support for this research.

E-ISSN: 2948-5231
Journal of Asian Geography, 2026, Volume 5 (Issue 2), 18-24
https://doi.org/10.36777/jag2026.5.2.2

Author contributions: Conceptualisation: Zhang Yibo and Mohd Amirul Mahamud; Methodology: Zhang Yibo and Mohd Amirul Mahamud; Literature search: Zhang Yibo; Data collection: Zhang Yibo; Data analysis: Zhang Yibo; Writing – original draft: Zhang Yibo; Writing – review and editing: Mohd Amirul Mahamud; Critical review: Mohd Amirul Mahamud; Supervision: Mohd Amirul Mahamud.

References

Abdulkareem, J. H., Pradhan, B., Sulaiman, W. N. A., & Jamil, N. R. (2018). Review of studies on hydrological modelling in Malaysia. *Modeling Earth Systems and Environment, 4*(4), 1577-1605. https://doi.org/10.1007/s40808-018-0509-y

de Brito, M. M., & Evers, M. (2016). Multi-criteria decision-making for flood risk management: A survey of the current state of the art. *Natural Hazards and Earth System Sciences, 16*(4), 1019-1033. https://doi.org/10.5194/nhess-16-1019-2016

Didan, K. (2015). *MOD13Q1 MODIS/Terra vegetation indices 16-day L3 global 250 m SIN grid V006* [Data set]. NASA EOSDIS Land Processes Distributed Active Archive Center.

Elvidge, C. D., Zhizhin, M., Ghosh, T., Hsu, F.-C., & Taneja, J. (2021). Annual time series of global VIIRS nighttime lights derived from monthly averages: 2012 to 2019. *Remote Sensing, 13*(5), 922. https://doi.org/10.3390/rs13050922

European Space Agency. (2021). *Copernicus DEM GLO-30* [Data set]. Copernicus Data Space Ecosystem.

Food and Agriculture Organization of the United Nations, & International Institute for Applied Systems Analysis. (2023). *Harmonized World Soil Database version 2.0* [Data set].

Fick, S. E., & Hijmans, R. J. (2017). WorldClim 2: New 1-km spatial resolution climate surfaces for global land areas. *International Journal of Climatology, 37*(12), 4302-4315. https://doi.org/10.1002/joc.5086

Hirabayashi, Y., Mahendran, R., Koirala, S., Konoshima, L., Yamazaki, D., Watanabe, S., Kim, H., & Kanae, S. (2013). Global flood risk under climate change. *Nature Climate Change, 3*(9), 816-821. https://doi.org/10.1038/nclimate1911

Jongman, B., Ward, P. J., & Aerts, J. C. J. H. (2012). Global exposure to river and coastal flooding: Long term trends and changes. *Global Environmental Change, 22*(4), 823-835. https://doi.org/10.1016/j.gloenvcha.2012.07.004

Kazakis, N., Kougias, I., & Patsialis, T. (2015). Assessment of flood hazard areas at a regional scale using an index-based approach and Analytic Hierarchy Process: Application in Rhodope-Evros region, Greece. *Science of the Total Environment, 538*, 555-563. https://doi.org/10.1016/j.scitotenv.2015.08.055

Lehner, B., & Grill, G. (2013). Global river hydrography and network routing: Baseline data and new approaches to study the world's large river systems. *Hydrological Processes, 27*(15), 2171-2186. https://doi.org/10.1002/hyp.9740

Malczewski, J. (2006). GIS-based multicriteria decision analysis: A survey of the literature. *International Journal of Geographical Information Science, 20*(7), 703-726. https://doi.org/10.1080/13658810600661508

Muzamil, S. A. H. B. S., Zainun, N. Y., Ajman, N. N., Sulaiman, N., Khahro, S. H., Rohani, M. M., Mohd, S. M. B., & Ahmad, H. (2022). Proposed framework for the flood disaster management cycle in Malaysia. *Sustainability, 14*(7), 4088. https://doi.org/10.3390/su14074088

OpenStreetMap contributors. (2025). *OpenStreetMap road network data for the Johor River Basin* [Data set]. https://www.openstreetmap.org

Rosmadi, H. S., Ahmed, M. F., Mokhtar, M. B., & Lim, C. K. (2023). Reviewing challenges of flood risk management in Malaysia. *Water, 15*(13), 2390. https://doi.org/10.3390/w15132390

Saaty, T. L. (1980). *The analytic hierarchy process: Planning, priority setting, resource allocation.* McGraw-Hill.

Shadiqe, J. (2025, December 12). Flood warning for low-lying areas in Johor from Dec 14-17. New Straits Times. https://www.nst.com.my/news/nation/2025/12/1336124/flood-warning-low-lying-areas-johor-dec-14%E2%80%9317

Sidek, L. M., Jaafar, A. S., Majid, W. H. A. W. A., Basri, H., Marufuzzaman, M., Fared, M. M., & Moon, W. C. (2021). High-resolution hydrological-hydraulic modeling of urban floods using InfoWorks ICM. *Sustainability, 13*(18), 10259. https://doi.org/10.3390/su131810259

Sirko, W., Kashubin, S., Ritter, M., Annkah, A., Bouchareb, Y. S. E., Dauphin, Y., Keysers, D., Neumann, M., Cisse, M., & Quinn, J. A. (2021). Continental-scale building detection from high-resolution satellite imagery. arXiv. https://doi.org/10.48550/arXiv.2107.12283

Souissi, D., Zouhri, L., Hammami, S., Msaddek, M. H., Zghibi, A., & Dlala, M. (2020). GIS-based MCDM-AHP modeling for flood susceptibility mapping of arid areas, southeastern Tunisia. *Geocarto International, 35*(9), 991-1017. https://doi.org/10.1080/10106049.2019.1566405

Tan, M. L., Ibrahim, A. L., Yusop, Z., Duan, Z., & Ling, L. (2015). Impacts of land-use and climate variability on hydrological components in the Johor River Basin, Malaysia. *Hydrological Sciences Journal, 60*(5), 873-889. https://doi.org/10.1080/02626667.2014.967246

Tatem, A. J. (2017). WorldPop, open data for spatial demography. *Scientific Data, 4*, 170004. https://doi.org/10.1038/sdata.2017.4

United Nations Office for Disaster Risk Reduction. (2022). *Global assessment report on disaster risk reduction 2022: Our world at risk - Transforming governance for a resilient future.* United Nations.

UNESCO Regional Office for Science and Technology for Southeast Asia. (1997). *Catalogue of rivers for Southeast Asia and the Pacific: Volume I - Mainland and insular Southeast Asia.* UNESCO.

Ward, P. J., Jongman, B., Weiland, F. S., Bouwman, A., van Beek, R., Bierkens, M. F. P., Ligtvoet, W., & Winsemius, H. C. (2013). Assessing flood risk at the global scale: Model setup, results, and sensitivity. *Environmental Research Letters, 8*(4), 044019. https://doi.org/10.1088/1748-9326/8/4/044019

WorldPop. (2024). *Global high-resolution population estimates and age-sex structures* [Data set]. University of Southampton. https://www.worldpop.org

Zanaga, D., Van De Kerchove, R., Daems, D., De Keersmaecker, W., Brockmann, C., Kirches, G., Wevers, J., Cartus, O., Santoro, M., Fritz, S., Lesiv, M., Herold, M., Tsendbazar, N. E., Xu, P., Ramoino, F., & Arino, O. (2022). *ESA WorldCover 10 m 2021 v200* [Data set]. Zenodo. https://doi.org/10.5281/zenodo.7254221